3-7-2008

Crystal structures of the Streptomyces coelicolor TetR-like protein ActR alone and in complex with actinorhodin or the actinorhodin biosynthetic precursor (S)-DNPA.

A R Willems

K Tahlan

T Taguchi

K Zhang

Z Z Lee

See next page for additional authors

Title:

Crystal structures of the *Streptomyces coelicolor* TetR-like protein ActR alone and in complex with actinorhodin or the actinorhodin biosynthetic precursor (*S*)-DNPA

Running title:

Structures of apo-ActR and ActR/ligand complexes

Authors:

Willems, A.R.[1]

Tahlan, K.[1]

Taguchi, T.[2]

Zhang, K.[1]

Lee, Z.Z.[1]

Ichinose, K.[2]

Junop, M.S.[1]

Nodwell, J.R.[1,3]

Affiliations:

[1]Department of Biochemistry and Biomedical Sciences, McMaster University, 1200 Main St. W, Hamilton, Ontario, L8N 3Z5, Canada.

[2]Research Institute of Pharmaceutical Sciences, Musashino University, Tokyo 202-8585, Japan.

[3]corresponding author: phone: (905) 525-9140 x27335; fax: (905) 522-9033; email: nodwellj@mcmaster.ca

Summary

Actinorhodin, an antibiotic produced by *Streptomyces coelicolor*, is exported from the cell by the ActA efflux pump. *actA* is divergently transcribed from *actR* which encodes a TetR-like transcriptional repressor. We showed previously that ActR represses transcription by binding to an operator from the *actA*/*actR* intergenic region. Importantly, actinorhodin itself or various actinorhodin biosynthetic intermediates can cause ActR to dissociate from its operator, leading to derepression. This suggests that ActR may mediate timely self-resistance to an endogenously produced antibiotic by responding to one of its biosynthetic precursors. Here we report the structural basis for this precursor-mediated derepression with crystal structures of homo-dimeric ActR by itself and in complex with either actinorhodin or the actinorhodin biosynthetic intermediate (*S*)-DNPA. The ligand-binding tunnel in each ActR monomer has a striking hydrophilic / hydrophobic / hydrophilic arrangement of surface residues that accommodate either one hexacyclic actinorhodin molecule or two back-to-back tricyclic (*S*)-DNPA molecules. Moreover, our work also reveals the strongest structural evidence to date that TetR-mediated antibiotic resistance may have been acquired from an antibiotic-producer organism.

Keywords: TetR transcriptional regulators; antibiotic export; X-ray crystal structures; *Streptomyces coelicolor*, protein ligand interactions

Introduction

TetR-like proteins comprise a large family of prokaryotic transcriptional regulators many of which function as repressors (reviewed in [1]). These proteins control genes that confer antibiotic resistance, as well as the biosynthesis of antibiotics and other bioactive small molecules, some of which act as signals to trigger cell differentiation. TetR-like proteins are believed to respond to small molecule ligands however the binding specificity of only a small number of them has been characterized to date.

The best characterized member of the family is TetR, an *E. coli* protein that confers resistance to the antibiotic tetracycline [2] by regulating the expression of the TetA tetracycline efflux pump [3]. In the absence of the drug, TetR binds tightly to its operator DNA in the intergenic region between the divergently transcribed *tetR* and *tetA* genes repressing expression of both genes [4; 5]. In the presence of tetracycline, however, TetR loses affinity for its operator, leading to *tetA* expression and export of the drug [6].

The mechanisms of repression and derepression have been elucidated with high resolution crystal structures for two TetR family proteins, *E. coli* TetR itself and QacR, a *Staphylococcus aureus* protein that confers resistance to multiple drugs including quaternary ammonium compounds [7; 8; 9; 10; 11; 12]. Both are homo-dimers, with an N-terminal helix-turn-helix containing DNA-binding domain (DBD) and a C-terminal ligand-binding domain (LBD). In their operator-bound repressing forms a single TetR homo-dimer binds DNA while two QacR homo-dimers bind DNA cooperatively. During derepression each of the two TetR monomers binds one tetracycline molecule (along with a magnesium ion) while only one of the QacR monomers binds up to two ligand molecules. In both cases, when ligand binds, localized secondary structure changes result in a movement of helix α6 located at the DBD/LBD interface. This increases the distance between the DBDs such that they are now too far apart to bind to their respective operator sites, causing the protein to fall off the DNA. There are only two other TetR-like proteins for which crystal structures exist with an identified ligand bound. EthR is a *Mycobacterium tuberculosis* repressor of *ethA*, a gene required for activation of the pro-

drug ethionamide. A structure of EthR purified from *E. coli* was solved in which a fortuitous ligand was identified as hexadecyl octanoate, while a structure of EthR purified from *M. smegmatis* had a similar compound [13]. Recently the structure was solved for the *Pseudomonas putida* protein TtgR, a repressor for the multidrug resistance export pump TtgABC, as a homo-dimer in complex with either two or three copies of various antibiotics and plant secondary metabolites [14].

The soil dwelling *Streptomyces* must survive in a very complex environment. Consistent with this, they synthesize a huge number and variety of antibiotics and other secondary metabolites [15; 16]. With 150 TetR-like proteins encoded in the *S. coelicolor* genome, this family of proteins undoubtedly plays critical roles in the transcriptional responses of this organism to a diverse array of intrinsic and extrinsic chemical signals [1].

The hexacyclic polyketide actinorhodin produced by *S. coelicolor* has 3*S*, 15*R* stereochemistry and is blue under alkaline conditions [17]. The biosynthesis of the actinorhodin core is accomplished by a type II polyketide synthase [18], leading to tricyclic intermediates such as (*S*)-DNPA that lack antibacterial activity, and are processed to give the mature hexacyclic molecule (Figure 1) [19]. Actinorhodin is primarily cell associated and it is transported out of the cell to achieve 'self resistance' in the form of γ-actinorhodin (a lactone of actinorhodin) [20]. Actinorhodin is exported from the cell by several putative transmembrane proteins encoded by *actA/actII-ORF2*, *actII-ORF3* and *actVA-ORF1* [21; 22; 23].

The transcription of the first two of these genes is repressed by a TetR-like protein, ActR/ActII-ORF1. Our recent studies have shown that derepression by ActR can be mediated not only by actinorhodin but also by actinorhodin biosynthetic intermediates or related compounds. This allows the cell to link a downstream function—actinorhodin export—to an upstream function that has not yet been completed—actinorhodin biosynthesis [24]. The interaction between a small molecule intermediate and a protein effector such as the one we have observed between (*S*)-DNPA and ActR represents a relatively novel type of interaction that may, however, be more widespread in nature [17;

[24]. Indeed, a similar type of interaction has been identified in the pathway for daunorubicin biosynthesis [24; 25; 26] and suggested (though not tested) for regulation of methylenomycin and phaseolotoxin synthesis as well [27; 28]. In order to understand the mechanism of ActR derepression, we have solved the crystal structures of ActR alone and in combination with both actinorhodin and the actinorhodin intermediate (*S*)-DNPA.

Abbreviations

(*S*)-DNPA: 4-dihydro-9-hydroxy-1-methyl-10-oxo-3-H-naphtho-[2,3-c]-pyran-3-(*S*)-acetic acid

DBD: DNA-binding domain

LBD: ligand-binding domain

SeMet: seleno-methionine

Results

The structure of apo-ActR

While we were able to obtain preliminary crystals using full length ActR we were not able to optimize them. However, ActR(30-259), in which residues N-terminal to the putative DBD are deleted, expressed well and was soluble so we used this construct for the remainder of our work. The first of these crystals belonged to the $P2_12_12_1$ space group and diffracted to 2.05 Å but we were unable to solve its structure using molecular replacement based on known TetR-like structures. Instead we obtained preliminary phases from seleno-methionine(SeMet)-containing crystals using single wavelength anomalous diffraction. We used the partially refined structure from one such crystal that belonged to the *P*2 space group and diffracted to 2.5 Å as a search model to solve the native structure by molecular replacement. Crystal parameters and refinement statistics for both the apo- and ligand-bound native crystals (see below) are listed in Table 1. Representative electron density of apo-ActR is shown in Figure 2A. We were able to model in several N-terminal vector-derived residues as alanines, three for chain A and one for chain B. Residues 246 to the C-terminus for chain A (or 244 to the C-terminus, for chain B), as well as residues 178-187 (or 179-188) between helices α8 and α9 (see below), were unstructured and not included in the model.

The structure shows that ActR forms an all-helical omega(Ω)-shaped homo-dimer typical of TetR family members [1] (Figure 3A). Each ActR monomer has three main segments (Figure 3B). Helices α1 through α3 and the N-terminus of α4 form the DBD. The remainder of α4, α5 through α8 and α11 form the core of the LBD. Finally, α9 and the kinked α10 form an arm that extends from the LBD of one monomer around the side of the opposing monomer's LBD. Each LBD has a tunnel that runs horizontally from the outside edge through the LBD core to the dimer centre, with the central termini of the two tunnels slightly offset from each other. Each tunnel creates a cavity of approximately 800 $Å^3$ within its respective monomer. Approximately half as much additional volume is created for each tunnel in the region between the monomers.

Structures of ActR/actinorhodin and ActR/(*S*)-DNPA

We also soaked crystals of apo-ActR with either actinorhodin or (*S*)-DNPA and solved the two ligand-bound structures to 3.05 Å and 2.30 Å respectively by molecular replacement (Table 1). Importantly, these structures clearly show several regions of electron density within the LBD tunnels. In the first such structure a continuous region of density running longitudinally down each tunnel reveals the presence of one actinorhodin molecule in each of chains A and B (Figure 2C). In contrast, disconnected regions of density in the second structure reveal the presence of two (*S*)-DNPA molecules in chain A (Figure 2D). A similar arrangement in chain B seems likely but the density in one of the two sites in chain B (the "proximal" site, see below) was too weak to confidently position the ligand. These structures allowed us to identify two ligand-binding sites in each tunnel, one "proximal" and one "distal" to the main dimer interface formed by helices α8 and α10. Each site thus binds either one tricyclic (*S*)-DNPA molecule or one tricyclic actinorhodin half-molecule (see Figure 1).

To investigate ActR motions we superimposed the core LBDs of all six ActR monomers. The loop between helices α6 and α7 (i.e. "loop 6/7") appears to play a critical role in TetR derepression [9; 10]. Our super-positions reveal firstly that this loop in ActR is indeed the most structurally variable region within the core LBD with apparently ligand-dependent and -independent motions up to 2.5 and 1.7 Å respectively (Figure 3B). Second, they show that the DBD can pivot around the C-terminus of helix α4 by up to 9° relative to the LBD in a ligand-independent manner, moving the far edge of the DBD up to 4 Å (Figure 3B). Third, we observe rotations up to 7° of one LBD relative to its dimeric partner through an axis running vertically through L162 (not shown). Notably, in each of our three dimers including apo-ActR the two DBD's are separated by 47-49 Å (measured between A66 Cα's; not shown), distances not compatible with binding to successive major grooves in undistorted DNA.

The residues surrounding the ligand-binding tunnel cluster into several distinct regions (Figure 4A). Most striking in terms of sheer numbers is the ring of seventeen hydrophobic residues that encircles the mid-point of the tunnel between the proximal and distal ligand-binding sites (Figure 4C). The only hydrophilic moiety here is the backbone carbonyl of M107. In contrast, the proximal and distal ligand-binding sites themselves are surrounded by a much higher proportion of hydrophilic side chains and backbone atoms (Figures 4B and D). Finally, a fourth surface region at the very proximal end of the tunnel is formed by five charged residues: D161 and, from the opposite monomer, E170, E173, R177, and R225. Together with three other side chains and a backbone carbonyl, these residues form an extensive hydrogen-bonding network (Figure 5A).

The relative positions of these regions within the tunnel provide a reasonable explanation for how both actinorhodin and (*S*)-DNPA bind to ActR. The longitudinal distribution of residues down the length of the tunnel forms a bilaterally symmetric pattern of polar, hydrophobic, and polar environments within the tunnel. This bilateral symmetry correlates well with the symmetry found in actinorhodin (Figure 4A): the central four non-hydrogen atoms of actinorhodin (atoms C9, C10, C10' and C9'; see Figure 1) constitute a hydrophobic core that is locked into position at the midpoint of the tunnel's central hydrophobic ring while actinorhodin's more polar oxygen-containing side groups situate its two molecular halves within the more polar proximal and distal ligand-binding sites. In a similar manner the bilateral symmetry of the binding tunnel also easily accommodates two (*S*)-DNPA molecules arranged in a back-to-back fashion (Figure 4A).

Discussion

ActR derepression by a biosynthetic intermediate

Importantly our structures provide a preliminary explanation for how it is that the actinorhodin precursor molecule, (*S*)-DNPA, can induce ActR derepression at least as well as actinorhodin itself [24]. In the proximal ligand-binding site (*S*)-DNPA and actinorhodin are almost super-imposable (Figure 4A). However, in the distal ligand-binding site actinorhodin and (*S*)-DNPA occupy distinct positions, with (*S*)-DNPA sitting over to the side of the tunnel (compare Figures 2C, 2D and 4A). It is not physically possible for the distal half of the actinorhodin molecule to reach this same position because of its covalent linkage to the proximal half of the molecule. We suggest therefore that (*S*)-DNPA may be able to interact so strongly with the ActR ligand binding cavity in part because of its greater positional degrees of freedom during docking relative to the covalently constrained actinorhodin.

Our work on the actinorhodin pathway here and elsewhere [24] constitutes proof-of-principle that ActR derepression by a biosynthetic intermediate is biochemically and structurally feasible. The present structures now provide a starting point from which to engineer ActR mutants that bind actinorhodin precursors but not actinorhodin itself. Tests to see whether such mutants can still initiate actinorhodin export *in vivo* in otherwise wild type cells would demonstrate unequivocally whether physiological levels of pathway intermediates can modulate ActR activity.

The mechanism of ActR derepression

Our crystal structures reveal a pendulum-like motion of the DBD and significant structural variability in loop 6/7, suggesting that the mechanism of ActR induction is similar to that of TetR. However, the movements we observe are to some extent ligand-independent and are not comparable in magnitude to those seen upon ligand binding by TetR or QacR. The simplest explanation for this is that the apo-ActR structure is already in the derepressed conformation and that ligand binding simply locks the protein into this

state. It is also possible that our ligand-bound structures are not fully derepressed forms of the protein. A similar situation was observed for a structure for TetR bound to tetracycline under non-derepressing conditions [29]. Even if ActR is not fully derepressed in our structures, however, we see both subtle changes and higher B-factors in the α6 region of ligand-bound ActR (not shown) that suggest that this region is important for induction.

ActR demonstrates a remarkable sensitivity to the chirality of the C3 and C15 positions of its tricyclic ligands. For example, while (*S*)-DNPA is able to reverse DNA binding by ActR, a very similar enantiomer, nanaomycin A, does not [24]. This could be because the non-inducing molecules fail to bind or because they bind but fail to induce. Intriguingly, within an extensive hydrogen-bonding network near the proximal ligand-binding site, residue R225 is firmly positioned and seems nearly poised to interact with the ligand's C1/2/3 carboxymethyl group (Figure 5). Such an interaction could be critical for ActR's discrimination between these related enantiomers.

Structural comparison of ActR with other TetR family proteins

ActR and TetR exhibit only a low level of primary amino acid sequence similarity (40% and 20% identity for the DBDs and LBDs respectively). Despite this, structure similarity searches with ActR and TetR demonstrate that these two proteins are more similar to each other than to nearly any of the other forty-plus TetR family members in the non-redundant structure database, including even other *Streptomyces* TetR-like proteins. For example, superpositions of TetR and ActR DBDs or their core LBDs yield RMSDs of 1.2 or 1.9 Å respectively. This is even more notable in light of the fact that the positions of the ligands within ActR are very similar to the position of tetracycline (also a polyketide derivative) in a structurally aligned TetR structure (Figures 6A and B). In contrast both the overall structures of QacR and EthR as well as the relative positions of ligands within these proteins differ significantly relative to both ActR and TetR (Figure 6B). It has long been speculated that antibiotic-producers such as *Streptomyces* are an evolutionary source of the antibiotic resistance observed in, for instance, clinically

relevant pathogens [17; 22; 30; 31; 32; 33]. The structural similarities between TetR and ActR, both in terms of global fold and in terms of ligand binding environment, lend further credence to this hypothesis.

Indeed, a growing number of biosynthetic enzyme structures [18; 34; 35; 36; 37] have reinforced the importance of actinorhodin in our understanding of polyketide synthesis. The ActR/ligand structures that we have reported here provide a valuable regulatory complement to these biosynthetic structures.

Materials and Methods

DNA manipulation

His6-TEV-ActR(2-259) and (30-259) were generated by PCR using oligos MJo2392 (GGAACCATGGCATCGCGAAGCGAGGAAGGG) and MJo2394 (GGAATCTAGA GGATCCTCATGACTCCGCGGGGG), or MJo2393 (GGAACCATGGCACCCCTG ACCCAGGACCG) and MJo2394, using pET28a-ActR [24] as the template, cutting with NcoI/XbaI and ligating into pPROEX HTa (Invitrogen) to produce plasmids pMJ4412 and pMJ4413 respectively. Clones were confirmed by sequencing.

Protein purification

ActR(30-259) was produced by transforming plasmid pMJ4413 into either *E. coli* B834(DE3) (Novagen) for producing SeMet-protein or BL21(DE3) (Novagen) for producing native protein. Overnight cultures were grown in LB at 37°C and diluted into 4 L of either SeMet-containing media as described [38] for the derivatized protein or LB media for the native protein. Cells were grown at 37°C to an OD_{600} of 0.6 to 0.8, induced with 1 mM IPTG, shifted to 16°C, grown overnight, harvested, resuspended in lysis buffer containing 20 mM Tris pH 8.0, 500 mM KCl, 10 mM imidazole, 2.8 mM β-mercaptoethanol, 1 mM benzamidine, 5 μg/mL leupeptin, 1 μM pepstatin, and 1 mM PMSF, lysed in a French pressure cell and clarified by centrifugation and filtration. ActR was purified on a Ni-NTA column, cleaved with His-tagged TEV protease, reapplied to the column, collected as a low imidazole eluate, buffer-exchanged into 50 mM KCl, 1 mM DTT, and 10 mM Tris pH 8.0 and concentrated. The resulting protein has a gly-ala-met-ala N-terminal extension.

Ligand preparation

Powdered actinorhodin and (*S*)-DNPA (4-dihydro-9-hydroxy-1-methyl-10-oxo-3-H-naphtho-[2,3-c]-pyran-3-(*S*)-acetic acid) were prepared as previously described [19; 39].

2 µL of 333 mM actinorhodin in 100% DMSO was mixed with 2 µL of 300 mM KOH followed by 36 µL of 100 mM Tris pH 8.7 to a concentration of 17 mM.

Protein crystallization

Crystals were grown in vapour diffusion experiments over 0.5 mL of 1.5 M $(NH_4)_2SO_4$. Apo-SeMet-ActR was crystallized in a sitting drop vapour diffusion experiment by mixing 12 µL of 5 mg/mL protein with 3 µL of mother liquor (10% PEG8000, 100 mM Tris pH 8.7, 200 mM CsCl, and 1.4% ethylene glycol) and 2 µL of 0.1M $MgCl_2$. The drop was incubated at 20°C for 7 days.

All native crystals were grown using hanging drop vapour diffusion experiments. A native apo-ActR crystal was obtained by mixing 0.7 µL of 30 mg/mL protein, 0.7 µL of mother liquor (30% PEG4000, 0.2 M sodium acetate and 100 mM Bis-Tris pH 6.5) and 0.14 µL of 0.1 M EDTA sodium salt. The drop was incubated at 20°C for 16 days with an overnight room temperature incubation from day 2 to day 3, with crystals appearing after 2 days. This crystal was used to solve the structure of apo-ActR.

A second apo-ActR crystal appeared after three days under the same conditions except that the additive was 1 M taurine instead of EDTA. After incubation at 20°C for 6 months, powdered (*S*)-DNPA was added directly to the crystallization drop and incubated overnight.

A third apo-ActR crystal was grown by mixing 0.7 µL of 30 mg/mL protein and 0.7 µL of mother liquor (30% PEG4000, 0.2 M sodium acetate and 70 mM Tris pH 8.5). The drop was incubated at 20°C and crystals appeared within 1 week. After 5 months, 0.3 µL of 17 mM actinorhodin was added to the drop and incubated at 20°C for 2 days.

No crystallization attempts were made with any other actinorhodin pathway biosynthetic intermediates, derivatives or shunt products.

Structure determination, model refinement and computational analysis

Except for the ActR/actinorhodin crystal, which was collected at beamline X12C, data sets were collected using the X8C beamline at the National Synchrotron Light Source, Brookhaven National Labs. Data sets were processed and scaled using *d*TREK*

[40]. A single apo-SeMet-ActR crystal was used to collect a SAD data set. Using *HYSS* [41; 42] all expected Se sites were located within the asymmetric unit. Experimental phases were improved by density modification using *CNS* [43]. An initial model was built and used as a search model for subsequent *MOLREP* [44] molecular replacement determinations of native apo and ligand-bound ActR data. Iterative rounds of model building and refinement for all ActR structures were carried out using *WinCoot* [45] and *REFMAC* [46] until R values and model geometry statistics fell within acceptable ranges (Table 1). The four dimers observed in the ActR/actinorhodin structure are all very similar to each other and thus chains A and B were used in all subsequent analyses as representative structures for this complex. Structural illustrations were generated with *PyMOL* [47]. Structural alignments were performed using helices α5, α7, α8 and α11. PDB files used in Figure 6 are the following: TetR: 2TCT [8]; QacR: 1JUP, 1JUS, 1JTY, 1JT6, 1JTX [11; 12] and EthR: 1U9N [13]. Tunnel volumes were calculated using *CASTp* [48].

Structure Deposition

Structural data for the apo-ActR, ActR/actinorhodin and ActR/(*S*)-DNPA structures have been deposited with the Protein Data Bank under the accession codes 2OPT, 3B6A and 3B6C respectively.

Acknowledgements

We would like to thank A. Davidson and P. Berti for helpful discussions. Ligand purification was supported by MEXT. HAITEKU (2004-2008) to K. I. The rest of this work was supported by CIHR grants MOP-53209 to MSJ and MOP-57684 to JRN.

References

1. Ramos, J. L., Martinez-Bueno, M., Molina-Henares, A. J., Teran, W., Watanabe, K., Zhang, X., Gallegos, M. T., Brennan, R. & Tobes, R. (2005). The TetR family of transcriptional repressors. *Microbiol Mol Biol Rev* 69, 326-56.
2. Hillen, W., Klock, G., Kaffenberger, I., Wray, L. V. & Reznikoff, W. S. (1982). Purification of the TET repressor and TET operator from the transposon Tn10 and characterization of their interaction. *J Biol Chem* 257, 6605-13.
3. Hillen, W. & Berens, C. (1994). Mechanisms underlying expression of Tn10 encoded tetracycline resistance. *Annu Rev Microbiol* 48, 345-69.
4. Bertrand, K. P., Postle, K., Wray, L. V., Jr. & Reznikoff, W. S. (1983). Overlapping divergent promoters control expression of Tn10 tetracycline resistance. *Gene* 23, 149-56.
5. Meier, I., Wray, L. V. & Hillen, W. (1988). Differential regulation of the Tn10-encoded tetracycline resistance genes tetA and tetR by the tandem tet operators O1 and O2. *Embo J* 7, 567-72.
6. Lederer, T., Takahashi, M. & Hillen, W. (1995). Thermodynamic analysis of tetracycline-mediated induction of Tet repressor by a quantitative methylation protection assay. *Anal Biochem* 232, 190-6.
7. Hinrichs, W., Kisker, C., Duvel, M., Muller, A., Tovar, K., Hillen, W. & Saenger, W. (1994). Structure of the Tet repressor-tetracycline complex and regulation of antibiotic resistance. *Science* 264, 418-20.
8. Kisker, C., Hinrichs, W., Tovar, K., Hillen, W. & Saenger, W. (1995). The complex formed between Tet repressor and tetracycline-Mg2+ reveals mechanism of antibiotic resistance. *J Mol Biol* 247, 260-80.
9. Orth, P., Cordes, F., Schnappinger, D., Hillen, W., Saenger, W. & Hinrichs, W. (1998). Conformational changes of the Tet repressor induced by tetracycline trapping. *J Mol Biol* 279, 439-47.
10. Orth, P., Schnappinger, D., Hillen, W., Saenger, W. & Hinrichs, W. (2000). Structural basis of gene regulation by the tetracycline inducible Tet repressor-operator system. *Nat Struct Biol* 7, 215-9.
11. Schumacher, M. A., Miller, M. C., Grkovic, S., Brown, M. H., Skurray, R. A. & Brennan, R. G. (2001). Structural mechanisms of QacR induction and multidrug recognition. *Science* 294, 2158-63.
12. Schumacher, M. A., Miller, M. C., Grkovic, S., Brown, M. H., Skurray, R. A. & Brennan, R. G. (2002). Structural basis for cooperative DNA binding by two dimers of the multidrug-binding protein QacR. *Embo J* 21, 1210-8.
13. Frenois, F., Engohang-Ndong, J., Locht, C., Baulard, A. R. & Villeret, V. (2004). Structure of EthR in a ligand bound conformation reveals therapeutic perspectives against tuberculosis. *Mol Cell* 16, 301-7.
14. Alguel, Y., Meng, C., Teran, W., Krell, T., Ramos, J. L., Gallegos, M. T. & Zhang, X. (2007). Crystal Structures of Multidrug Binding Protein TtgR in Complex with Antibiotics and Plant Antimicrobials. *J Mol Biol* 369, 829-40.
15. Bentley, S. D., Chater, K. F., Cerdeno-Tarraga, A. M., Challis, G. L., Thomson, N. R., James, K. D., Harris, D. E., Quail, M. A., Kieser, H., Harper, D., Bateman,

A., Brown, S., Chandra, G., Chen, C. W., Collins, M., Cronin, A., Fraser, A., Goble, A., Hidalgo, J., Hornsby, T., Howarth, S., Huang, C. H., Kieser, T., Larke, L., Murphy, L., Oliver, K., O'Neil, S., Rabbinowitsch, E., Rajandream, M. A., Rutherford, K., Rutter, S., Seeger, K., Saunders, D., Sharp, S., Squares, R., Squares, S., Taylor, K., Warren, T., Wietzorrek, A., Woodward, J., Barrell, B. G., Parkhill, J. & Hopwood, D. A. (2002). Complete genome sequence of the model actinomycete *Streptomyces coelicolor* A3(2). *Nature* 417, 141-7.

16. Ikeda, H., Ishikawa, J., Hanamoto, A., Shinose, M., Kikuchi, H., Shiba, T., Sakaki, Y., Hattori, M. & Omura, S. (2003). Complete genome sequence and comparative analysis of the industrial microorganism *Streptomyces avermitilis*. *Nat Biotechnol* 21, 526-31.
17. Hopwood, D. A. (2007). How do antibiotic-producing bacteria ensure their self-resistance before antibiotic biosynthesis incapacitates them? *Mol Microbiol* 63, 937-40.
18. Keatinge-Clay, A. T., Maltby, D. A., Medzihradszky, K. F., Khosla, C. & Stroud, R. M. (2004). An antibiotic factory caught in action. *Nat Struct Mol Biol* 11, 888-93.
19. Taguchi, T., Itou, K., Ebizuka, Y., Malpartida, F., Hopwood, D. A., Surti, C. M., Booker-Milburn, K. I., Stephenson, G. R. & Ichinose, K. (2000). Chemical characterisation of disruptants of the Streptomyces coelicolor A3(2) actVI genes involved in actinorhodin biosynthesis. *J Antibiot (Tokyo)* 53, 144-52.
20. Bystrykh, L. V., Fernandez-Moreno, M. A., Herrema, J. K., Malpartida, F., Hopwood, D. A. & Dijkhuizen, L. (1996). Production of actinorhodin-related "blue pigments" by *Streptomyces coelicolor* A3(2). *J Bacteriol* 178, 2238-44.
21. Caballero, J. L., Martinez, E., Malpartida, F. & Hopwood, D. A. (1991). Organisation and functions of the actVA region of the actinorhodin biosynthetic gene cluster of *Streptomyces coelicolor*. *Mol Gen Genet* 230, 401-12.
22. Caballero, J. L., Malpartida, F. & Hopwood, D. A. (1991). Transcriptional organization and regulation of an antibiotic export complex in the producing *Streptomyces* culture. *Mol Gen Genet* 228, 372-80.
23. Fernandez-Moreno, M. A., Caballero, J. L., Hopwood, D. A. & Malpartida, F. (1991). The act cluster contains regulatory and antibiotic export genes, direct targets for translational control by the bldA tRNA gene of *Streptomyces*. *Cell* 66, 769-80.
24. Tahlan, K., Ahn, S. K., Sing, A., Bodnaruk, T. D., Willems, A. R., Davidson, A. R. & Nodwell, J. R. (2007). Initiation of actinorhodin export in *Streptomyces coelicolor*. *Mol Microbiol* 63, 951-61.
25. Otten, S. L., Ferguson, J. & Hutchinson, C. R. (1995). Regulation of daunorubicin production in *Streptomyces peucetius* by the dnrR2 locus. *J Bacteriol* 177, 1216-24.
26. Jiang, H. & Hutchinson, C. R. (2006). Feedback regulation of doxorubicin biosynthesis in *Streptomyces peucetius*. *Res Microbiol* 157, 666-74.
27. Hobbs, G., Obanye, A. I., Petty, J., Mason, J. C., Barratt, E., Gardner, D. C., Flett, F., Smith, C. P., Broda, P. & Oliver, S. G. (1992). An integrated approach to studying regulation of production of the antibiotic methylenomycin by *Streptomyces coelicolor* A3(2). *J Bacteriol* 174, 1487-94.

28. Lopez-Lopez, K., Hernandez-Flores, J. L., Cruz-Aguilar, M. & Alvarez-Morales, A. (2004). In *Pseudomonas syringae pv. phaseolicola*, expression of the argK gene, encoding the phaseolotoxin-resistant ornithine carbamoyltransferase, is regulated indirectly by temperature and directly by a precursor resembling carbamoylphosphate. *J Bacteriol* 186, 146-53.
29. Orth, P., Saenger, W. & Hinrichs, W. (1999). Tetracycline-chelated Mg2+ ion initiates helix unwinding in Tet repressor induction. *Biochemistry* 38, 191-8.
30. Walker, M. S. & Walker, J. B. (1970). Streptomycin biosynthesis and metabolism. Enzymatic phosphorylation of dihydrostreptobiosamine moieties of dihydro-streptomycin-(streptidino) phosphate and dihydrostreptomycin by *Streptomyces* extracts. *J Biol Chem* 245, 6683-9.
31. Watanabe, T. (1971). The problems of drug-resistant pathogenic bacteria. The origin of R factors. *Ann N Y Acad Sci* 182, 126-40.
32. Benveniste, R. & Davies, J. (1973). Aminoglycoside antibiotic-inactivating enzymes in actinomycetes similar to those present in clinical isolates of antibiotic-resistant bacteria. *Proc Natl Acad Sci U S A* 70, 2276-80.
33. D'Costa, V. M., McGrann, K. M., Hughes, D. W. & Wright, G. D. (2006). Sampling the antibiotic resistome. *Science* 311, 374-7.
34. Crump, M. P., Crosby, J., Dempsey, C. E., Parkinson, J. A., Murray, M., Hopwood, D. A. & Simpson, T. J. (1997). Solution structure of the actinorhodin polyketide synthase acyl carrier protein from *Streptomyces coelicolor* A3(2). *Biochemistry* 36, 6000-8.
35. Sciara, G., Kendrew, S. G., Miele, A. E., Marsh, N. G., Federici, L., Malatesta, F., Schimperna, G., Savino, C. & Vallone, B. (2003). The structure of ActVA-Orf6, a novel type of monooxygenase involved in actinorhodin biosynthesis. *Embo J* 22, 205-15.
36. Hadfield, A. T., Limpkin, C., Teartasin, W., Simpson, T. J., Crosby, J. & Crump, M. P. (2004). The crystal structure of the actIII actinorhodin polyketide reductase: proposed mechanism for ACP and polyketide binding. *Structure* 12, 1865-75.
37. Korman, T. P., Hill, J. A., Vu, T. N. & Tsai, S. C. (2004). Structural analysis of actinorhodin polyketide ketoreductase: cofactor binding and substrate specificity. *Biochemistry* 43, 14529-38.
38. Hendrickson, W. A., Horton, J. R. & LeMaster, D. M. (1990). Selenomethionyl proteins produced for analysis by multiwavelength anomalous diffraction (MAD): a vehicle for direct determination of three-dimensional structure. *Embo J* 9, 1665-72.
39. Taguchi, T., Ebizuka, Y., Hopwood, D. A. & Ichinose, K. (2001). A new mode of stereochemical control revealed by analysis of the biosynthesis of dihydrogranaticin in *Streptomyces violaceoruber* Tu22. *J Am Chem Soc* 123, 11376-80.
40. Pflugrath, J. W. (1999). The finer things in X-ray diffraction data collection. *Acta Crystallogr D Biol Crystallogr* 55, 1718-25.
41. Adams, P. D., Grosse-Kunstleve, R. W., Hung, L. W., Ioerger, T. R., McCoy, A. J., Moriarty, N. W., Read, R. J., Sacchettini, J. C., Sauter, N. K. & Terwilliger, T. C. (2002). PHENIX: building new software for automated crystallographic structure determination. *Acta Crystallogr D Biol Crystallogr* 58, 1948-54.

42. Grosse-Kunstleve, R. W. & Adams, P. D. (2003). Substructure search procedures for macromolecular structures. *Acta Crystallogr D Biol Crystallogr* 59, 1966-73.
43. Brunger, A. T., Adams, P. D., Clore, G. M., DeLano, W. L., Gros, P., Grosse-Kunstleve, R. W., Jiang, J. S., Kuszewski, J., Nilges, M., Pannu, N. S., Read, R. J., Rice, L. M., Simonson, T. & Warren, G. L. (1998). Crystallography & NMR system: A new software suite for macromolecular structure determination. *Acta Crystallogr D Biol Crystallogr* 54, 905-21.
44. Vagin, A. & Teplyakov, A. (1997). MOLREP: An automated program for molecular replacement. *J. Appl. Crystallogr.* 30, 1022-1025.
45. Emsley, P. & Cowtan, K. (2004). Coot: model-building tools for molecular graphics. *Acta Crystallogr D Biol Crystallogr* 60, 2126-32.
46. Murshudov, G. N., Vagin, A. A. & Dodson, E. J. (1997). Refinement of macromolecular structures by the maximum-likelihood method. *Acta Crystallogr D Biol Crystallogr* 53, 240-55.
47. DeLano, W. L. (2002). The PyMOL Molecular Graphics System, Palo Alto, CA, USA.
48. Binkowski, T. A., Naghibzadeh, S. & Liang, J. (2003). CASTp: Computed Atlas of Surface Topography of proteins. *Nucleic Acids Res* 31, 3352-5.

Figure Legends

Figure 1. Actinorhodin biosynthesis and export. An initial polyketide is transformed via multiple enzyme-catalyzed steps into (*S*)-DNPA and, eventually, actinorhodin, which is exported from the cell. The proposed mechanism of export regulation by actinorhodin and (*S*)-DNPA is supported by recent studies that show that ActR can be derepressed by these compounds [24]. Numbering of selected carbon atoms is indicated. The dashed line within actinorhodin indicates its internal bilateral symmetry.

Figure 2. Electron densities in the ActR ligand-binding region. All figures are F_o-F_c omit maps calculated with the drawn atoms removed. (A) Apo-ActR map, drawn within 1.7 Å of residues 125-133 contoured at 2 sigma. (B-D) The ligand-binding region in (B) apo-ActR, (C) ActR/actinorhodin, and (D) ActR/(*S*)-DNPA. Maps are shown within 2.2 Å of the ligands contoured at 1.3 sigma. Residues N-terminal to α5 have been removed for clarity. Ligand binding sites are named according to their positions relative to the interface between the α8/α11 surfaces of the apposing monomers. All views here and elsewhere are of chain A unless stated otherwise and, when coloured by atom, have O, N and S coloured red, blue and yellow respectively, with C coloured variously as appropriate.

Figure 3. The overall structure and movements of ActR. (A) The structure of apo-ActR. The various protein regions are coloured as in part B. Chain B has muted colours and primes added to helix names. (B) Relative movements within the ActR monomer. The chain A structures are shown in the same orientation as in part A. The different protein regions are coloured and labeled. All six ActR monomers were superpositioned using the LBDs. Positions of corresponding atoms in the different structures are connected by black lines. The rigidity of the LBD core is demonstrated by the short black lines in this domain. In contrast, the relative mobilities of the arm, loop 6/7, and the DBD are emphasized by the longer black lines in these regions. In particular, the arrow highlights the pendulum-like motion seen in the DBD relative to the LBD.

Figure 4. ActR structural features near the ligand-binding sites.
(A) "Side" view of the ligand-binding tunnel. The figure shows the internal molecular surface of the tunnel from chain A of the ActR/(*S*)-DNPA structure, showing the positions of (*S*)-DNPA and an actinorhodin molecule from a structurally superimposed ActR/actinorhodin structure. The protein surface is coloured by region.
(B-D) "End-on" views of the (B) proximal polar, (C) central hydrophobic and (D) distal polar regions in the ligand-binding tunnel. Residues and surface representations are drawn. For clarity only the (B) proximal three, (C) central four and (D) distal three rings of the ligands are drawn. Protein Cα carbons are drawn as spheres; side chain and backbone atoms are drawn as thick and thin cylinders respectively. Residues from chain B are indicated with "(B)". Residues contributing only backbone carbonyl or amide atoms are indicated with "_O" and "_N" respectively. Asterisks indicate residues that are also part of the hydrogen-bonding network shown in Figure 5.

Figure 5. The hydrogen-bonding network near the proximal ligand-binding site. Side chains and one backbone carbonyl group that form a hydrogen-bonding network in the ActR/(*S*)-DNPA structure are shown. The molecular protein surface of the proximal end of the ligand-binding tunnel of chain A is shown, as is the position of the proximal (*S*)-DNPA molecule. Note the proximity of the ligand carboxymethyl group and R225.

Figure 6. Structural comparisons of several TetR-like proteins bound to their ligands.
(A) Details of the ligand-binding regions in ActR/actinorhodin and TetR/7-chlor-tetracycline (pdb: 2TCT). Corresponding structural features are coloured the same. Note the positional similarity between ActR P130 and TetR P105 for which the side chains are shown. The grey sphere in the TetR structure is a magnesium ion. (B) A comparison of protein/ligand interactions for four TetR family proteins [8; 11; 12; 13]. The core LBD for one monomer of each of the four proteins is shown as a ribbon, while the other monomer of each is shown as a thin line. The QacR structure shows ligands from numerous structures superimposed within one representative protein domain. Note how ActR shows significantly greater similarity in terms of both protein structure and ligand position to TetR as compared to either of the others.

Table

Table 1. Crystallographic data and refinement statistics. Data for the highest resolution shell are shown in parentheses.

	ActR	ActR /actinorhodin	ActR /(*S*)-DNPA
Solution method	molec. replacmt.	molec. replacement	molec. replacement
Data collection			
Wavelength (Å)	1.1	1.1	1.1
Space group	$P2_12_12_1$	$P1$	$P2_12_12_1$
Unit-cell parameters (Å, °)	a = 55.6, b = 80.0, c = 104.0, $\alpha = \beta = \gamma = 90$	a = 57.9, b = 79.0, c = 107.2, α = 89.6, β = 89.9, γ = 89.9	a = 56.0, b = 79.4, c = 103.5, $\alpha = \beta = \gamma = 90$
No. of molecules in ASU	2	8	2
Resolution range (Å)	63.37-1.96 (2.03-1.96)	37.12-3.05 (3.16-3.05)	49.23-2.30 (2.38-2.30)
Unique reflections	34133	34551	19458
Data redundancy	7.20 (7.20)	1.88 (1.90)	4.63 (4.47)
Completeness (%)	99.9 (100.0)	96.0 (97.0)	92.1 (95.7)
$I/\sigma(I)$	34.60 (3.85)	10.6 (2.4)	17.6 (4.3)
R_{merge} (%)	5.5 (54.3)	5.5 (26.9)	4.7 (21.1)
Model and refinement			
Resolution range (Å)	63.37-2.05 (2.10-2.05)	37.12-3.05 (3.13-3.05)	41.85-2.30 (2.36-2.30)
Cutoff criterion	$\|F\|/\sigma(F) > 1$	$\|F\|/\sigma(F) > 1$	$\|F\|/\sigma(F) > 4$
R_{work} (%)	19.5 (22.9)	25.6 (34.2)	24.23 (32.4)
R_{free} (%)	24.7 (33.6)	28.8 (38.3)	28.49 (29.3)
No. of reflections	28206 (1507)	29797 (939)	14054 (743)
No. of amino-acids/atoms	431/3247	1720/13452	405/3292
Modeled residues	A:27-177,188-245	A,C,E,G:28-179,183-245	A:28-177,190-241
(chains:residues)	B:29-178,189-243	B,D,F,H:29-243	B:29-177,189-242
No. of waters	318	0	147
R.m.s.d. bond lengths (Å)	0.017	0.013	0.006
R.m.s.d. bond angles (°)	1.594	1.579	0.867
Average *B* factor (Å^2)	44.9	51.5	84.2

Figure

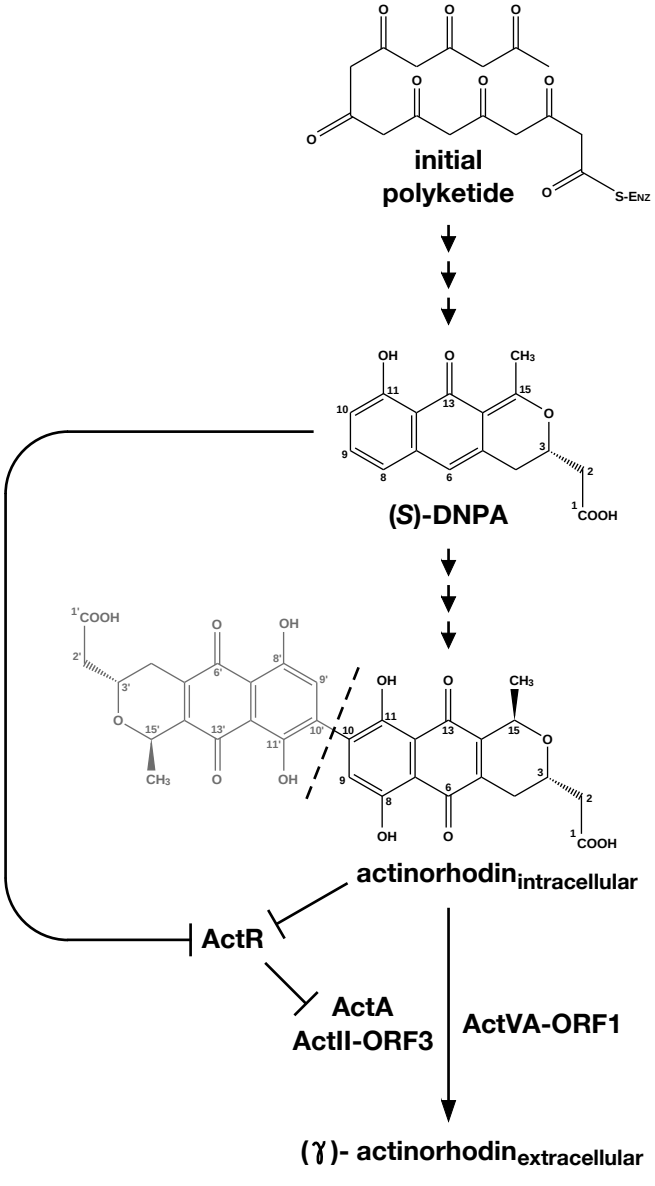
initial
polyketide
S-ENZ
(S)-DNPA
actinorhodin intracellular
ActR
ActA
ActII-ORF3
ActVA-ORF1
(γ)- actinorhodin extracellular

Figure

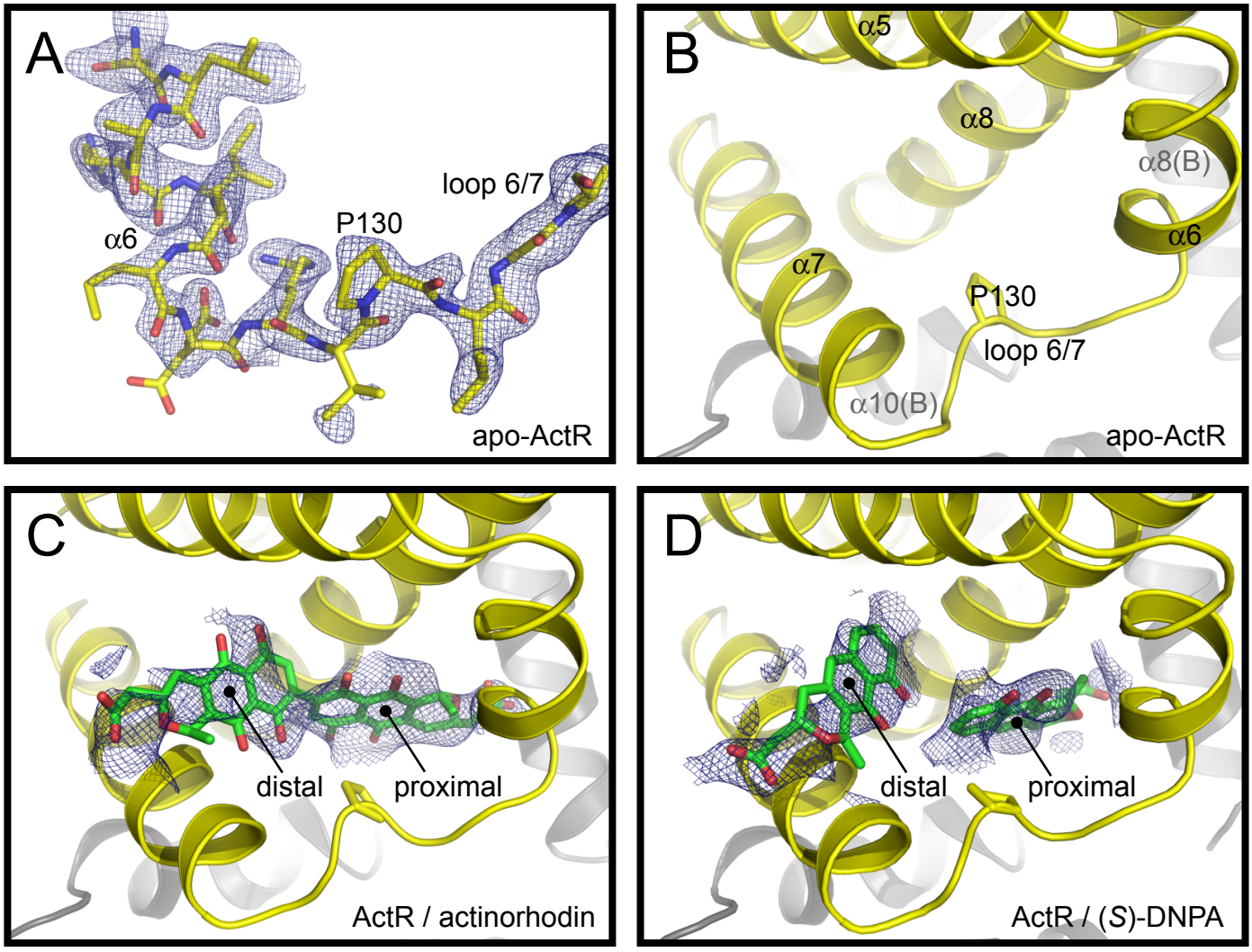
A
α6
P130
loop 6/7
apo-ActR
B
α5
α8
α8(B)
α6
α7
P130
loop 6/7
α10(B)
apo-ActR
C
distal
proximal
ActR / actinorhodin
D
distal
proximal
ActR / (S)-DNPA

Figure

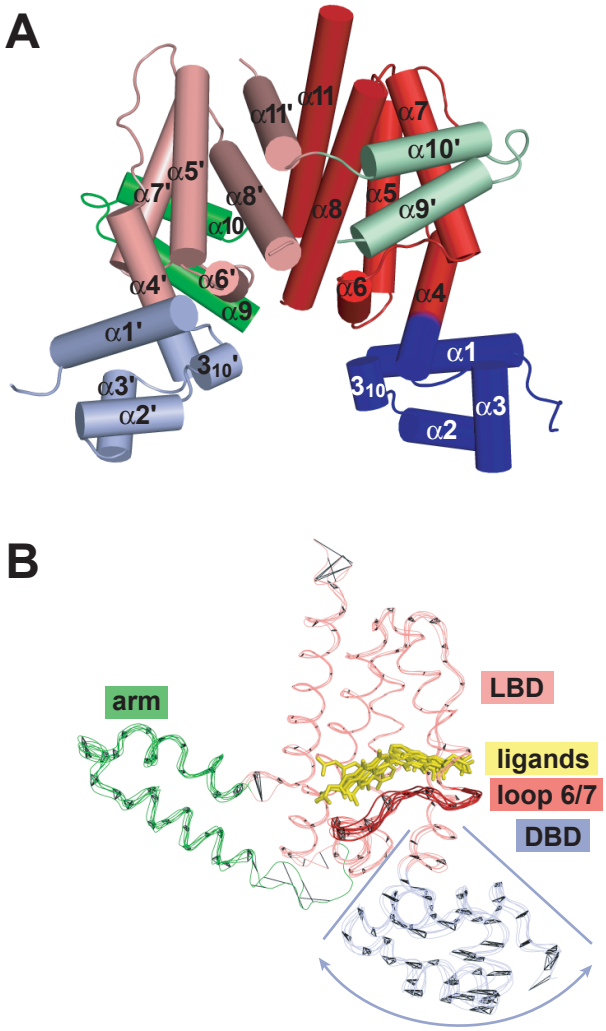
A
α11'
α11
α7
α10'
α5'
α7'
α8'
α5
α9'
α10
α8
α4'
α6'
α6
α4
α9
α1'
α1
3₁₀'
3₁₀
α3'
α3
α2'
α2
B
arm
LBD
ligands
loop 6/7
DBD

Figure

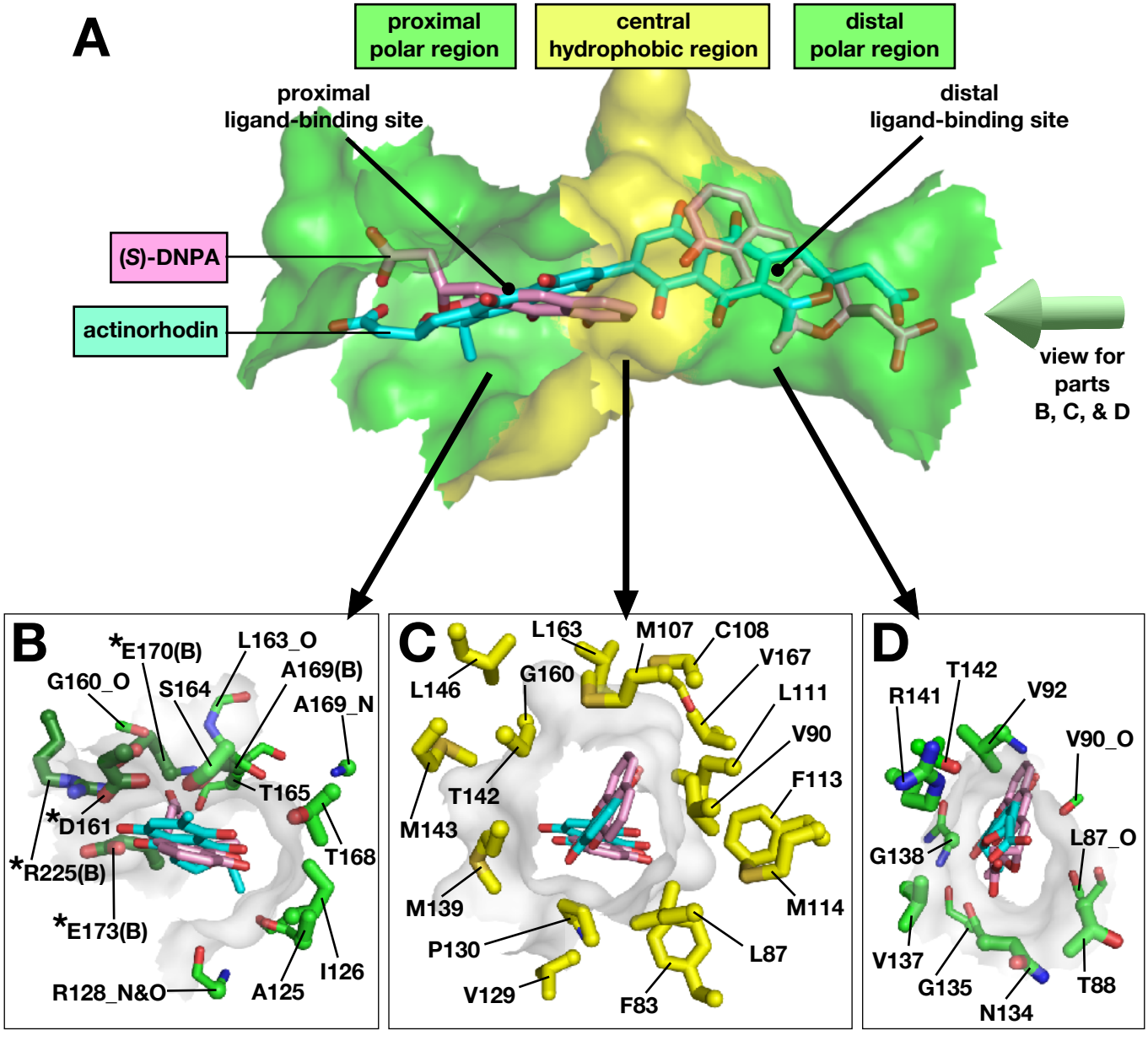
A
proximal polar region
central hydrophobic region
distal polar region
proximal ligand-binding site
distal ligand-binding site
(S)-DNPA
actinorhodin
view for parts B, C, & D
B
*E170(B)
L163_O
A169(B)
G160_O
S164
A169_N
T165
*D161
T168
*R225(B)
*E173(B)
I126
R128_N&O
A125
C
L163
M107
C108
V167
G160
L146
L111
V90
T142
F113
M143
M114
M139
L87
P130
V129
F83
D
T142
R141
V92
V90_O
L87_O
G138
V137
G135
T88
N134

Figure

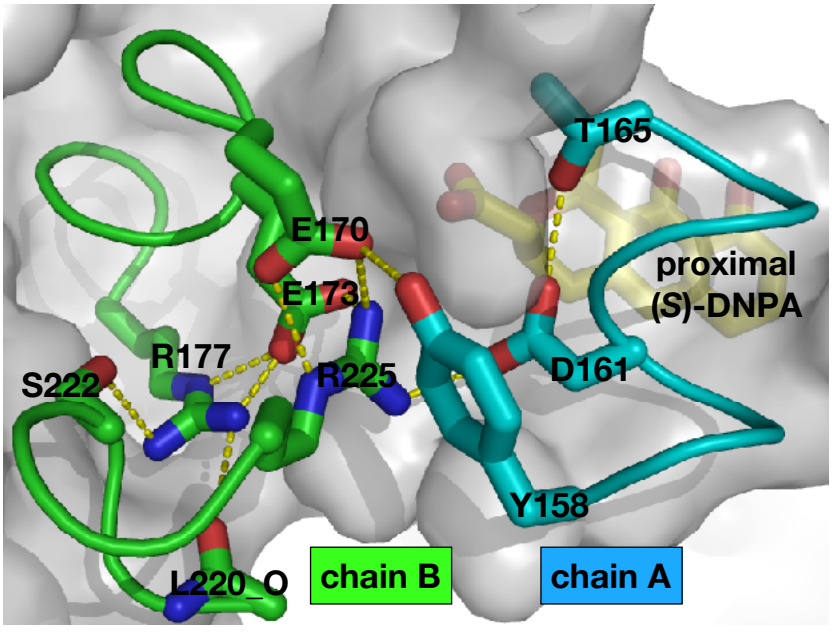
T165
E170
E173
proximal
(S)-DNPA
R177
S222
R225
D161
Y158
L220_O
chain B
chain A

Figure

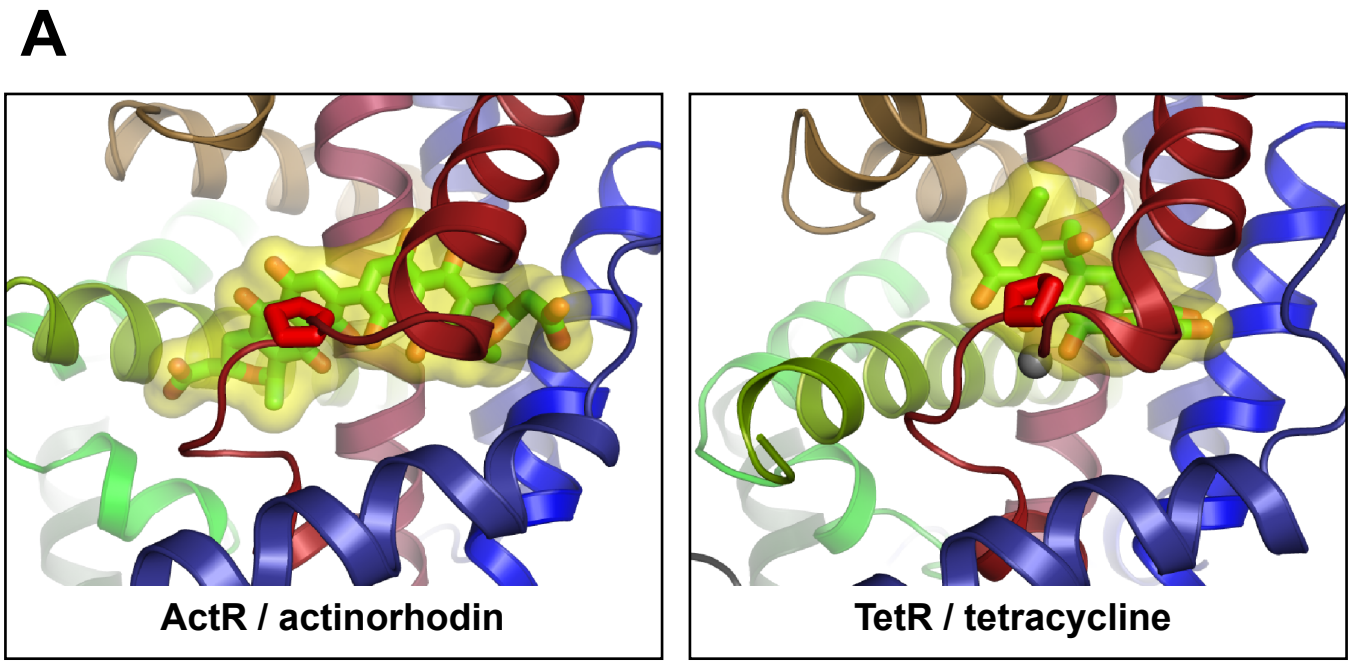
A
ActR / actinorhodin
TetR / tetracycline
B
ActR/
actinorhodin
TetR/
tetracycline
QacR/
ligands
EthR/
HexOc